Electronic Supplementary Information

Band-like transporting and thermally durable V-shaped organic semiconductors with a phenyl key block

Chizuru Sawabe,[a] Shohei Kumagai,[a] Masato Mitani,[a] Hiroyuki Ishii,[b] Masakazu Yamagishi,[c] Hajime Sagayama,[d] Reiji Kumai,[d] Hiroyasu Sato,[e] Jun Takeya[a,f,g] and Toshihiro Okamoto[*,a,f,h]

[a] Material Innovation Research Center (MIRC) and Department of Advanced Materials Science, School of Frontier Sciences, The University of Tokyo, 5-1-5 Kashiwanoha, Kashiwa, Chiba 277-8561, Japan.
[b] Department of Applied Physics, Faculty of Pure and Applied Sciences, University of Tsukuba, 1-1-1 Tennodai, Tsuku-ba, Ibaraki 305-8573, Japan.
[c] National Institute of Technology, Toyama College, 13 Hongo-machi, Toyama, Toyama 939-8630, Japan.
[d] Condensed Matter Research Centre (CMRC) and Photon Factory, Institute of Materials Structure Science, High Energy Accelerator Research Organization (KEK), Tsukuba 305-0801, Japan.
[e] Rigaku Corporation, 3-9-12 Matsubara-cho, Akishima, Tokyo 196-8666, Japan.
[f] National Institute of Advanced Industrial Science and Technology (AIST)-University of Tokyo Advanced Operando-Measurement Technology Open Innovation Laboratory (OPERANDO-OIL), AIST, 5-1-5 Kashiwanoha, Kashiwa, Chiba 277-8561, Japan.
[g] International Center for Materials Nanoarchitectonics (MANA), National Institute for Materials Science (NIMS), 1-1 Namiki, Tsukuba 205-0044, Japan.
[h] PRESTO, JST, 4-1-8 Honcho, Kawaguchi, Saitama 332-0012, Japan.

*Correspondence and requests for materials should be addressed to
tokamoto@k.u-tokyo.ac.jp

Contents

1. Synthesis

1.1 Materials

Tetrakis(triphenylphosphine)palladium (0) ($Pd(PPh_3)_4$), [1,1'-bis(diphenylphosphino)ferrocene] palladium(II) dichloride dichloromethane adduct ($PdCl_2(dppf)\cdot CH_2Cl_2$), 1-decyne, 1-bromo-4-iodobenzene, 4-bromophenol and 1-bromononane were purchased from TCI. *i*-PrMgBr, zinc chloride in tetrahydrofuran (THF) solution, magnesium turnings, 1,2-dibromoethane, 1,10-phenanthroline and cesium carbonate were purchased from WAKO chemicals. Lithium chloride (LiCl) in THF solution, iodine chloride (ICl) in CH_2Cl_2 solution and cupper iodide (CuI) were purchased from Sigma-Aldrich. *n*-BuLi in hexane, potassium carbonate, and all anhydrous solvents were purchased from KANTO chemicals.

1.2 General for Synthesis and Characterization

All reactions were carried out under an atmosphere of argon. Air- or moisture-sensitive liquids and solutions were transferred via a syringe or a Teflon cannula. Analytical thin-layer chromatography (TLC) was performed on glass plates with silica gel containing a fluorescent indicator (Merck PLC Silica gel 60 F254, 1 mm). TLC plates were visualized by exposure to ultraviolet lamp (254 nm and 365 nm) and by dipping in 10% phosphomolybdic acid in ethanol and heating by a heat gun. Flash column chromatography was performed on Biotage SNAP Ultra (HP-Sphere^{TM} 25 μm). All NMR spectra were recorded on a ECS400 spectrometer. Chemical shifts are reported in parts per million (ppm, δ scale) from residual protons in the deuterated solvent for ^{1}H NMR (δ 7.26 ppm for chloroform, 5.93 ppm for 1,1,2,2-tetrachloroethane (TCE)). The data were presented in the following format: chemical shift, multiplicity (s = singlet, d = doublet, t = triplet, m = multiplet), coupling constant in Hertz (Hz), signal area integration in natural numbers, assignment (italic). Mass spectra were measured on a Thermo Fisher SCIENTIFIC LTQ Orbitrap XL. Elemental analysis was collected on a J-Science Lab JM10 MICRO CORDER.

1.3 Experimental Procedure

3,9-Bis(trimethylsilyl)dinaphtho[2,3-b:2',3'-d] thiophene (**2**)

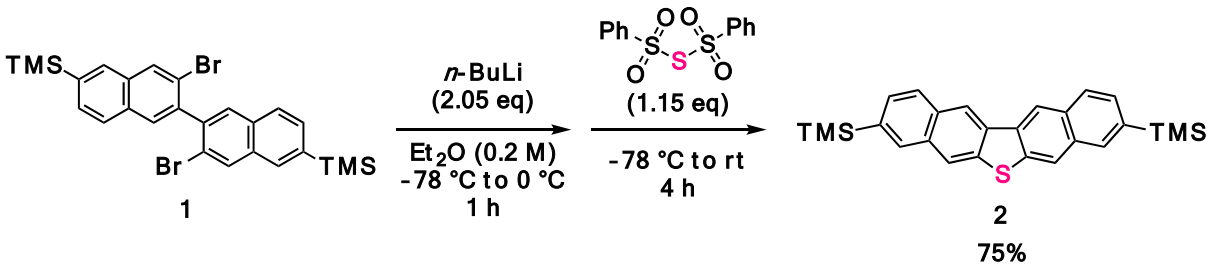

n-BuLi in hexane (1.64 M, 2.90 mL, 4.75 mmol, 2.05 eq.) was added to a solution of 3,3'-dibromo-6,6'-bis(trimethylsilyl)-2,2'-binaththalene (**1**) (1.29 g, 2.32 mmol) in diethylether (11.6 mL, 0.2 M) at –78 °C. After stirring at 0 °C for 1 h, benzenesulfonic thioanhydride (838.5 mg, 2.67 mmol, 1.15 eq.) suspended in THF (2.67 mL, 1 M) was added by a cannula at –78 °C, and the resulting mixture was stirred at ambient temperature for 4 h. To the reaction mixture, MeOH was added and the solids were collected by filtration. The crude material was purified by silica gel column chromatography (hexane: CH_2Cl_2 = 100:0 to 95:5) to afford the titled compound **2** (746.8 mg, 75% yield) as a white solid. ^{1}H-NMR (400 MHz, $CDCl_3$): δ 0.38 (s, 18H, Si(C*H*$_3$)$_3$), 7.64 (d, J = 8.0 Hz, 2H, Ar*H*), 8.03 (d, J = 8.4 Hz, 2H, Ar*H*), 8.06 (s, 2H, Ar*H*), 8.71 (s, 2H, Ar*H*).

3,9-Diiodedinaphtho[2,3-b:2',3'-d] thiophene (**I–DNT–VW**)

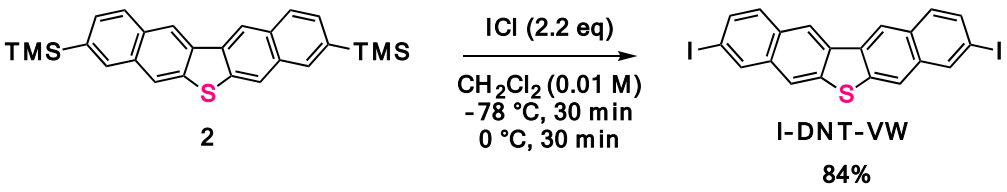

To a suspension of 3,9-bis(trimethylsilyl)dinaphtho[2,3-*b*:2',3'-*d*] thiophene (**2**) (645.5 mg, 1.51 mmol) in dichloromethane (150.6 mL, 0.01 M) was added ICl in dichloromethane (1.0 M, 3.31 mL, 3.31 mmol, 2.2 eq.) at –78 °C. The resulting mixture was stirred at –78 °C and 0 °C for each 30 min . After the reaction was quenched with a saturated sodium hydrosulfite aqueous solution, the resulting yellow precipitates were collected by filtration and washed by MeOH. The resulting material was dissolved in 1,2-dichlorobenzene at 120 °C and subjected to

subsequent filtrations through a short pad of silica gel and celite. After reducing the solvent *in vacuo*, the yellow solid was purified by recrystallization from 1,2-dichlorobenzene to afford the key precursor, **I–DNT–VW** (542.2 mg, 1.01 mmol, 67% yield) as a yellow solid. The solvent was removed *in vacuo*, and further purified by recrystallization from 1,2-dichlorobenzene to afford the pure product (136.0 mg, 0.25 mmol, 17% yield). Total yield: 84%. ^{1}H-NMR (400 MHz, TCE-d2, 100 °C): δ 7.75 (s, 2H, Ar*H*), 7.75 (s, 2H, Ar*H*), 8.08 (s, 2H, Ar*H*), 8.30 (s, 2H, Ar*H*), 8.62 (s, 2H, Ar*H*).

3,9-Bilphenyl dinaphtho[2,3-b:2',3'-d] thiophene (**Ph–DNT–VW**)

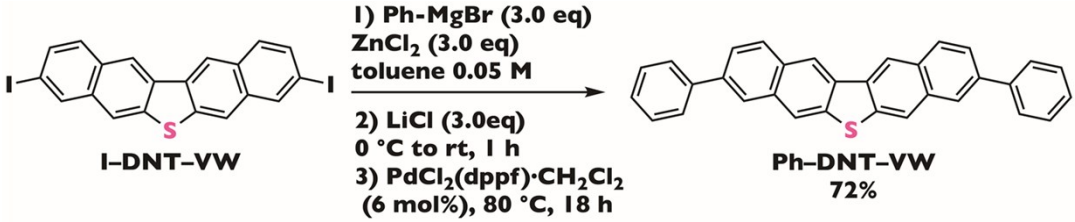

To a mixture of phenylmagnesium bromide in THF (1.0 M, 1.71 mL, 1.71 mmol, 3.0 eq.) and toluene (12.3 mL, 0.05 M) was added $ZnCl_2$ in THF (1.0 M, 1.71 mL, 1.71 mmol, 3.0 eq.) at the ambient temperature. After stirring 1 h, LiCl in THF (0.5 M, 3.40 mL, 1.70 mmol, 3.0 eq.) was added to the white suspension at 0 °C. After warming to the ambient temperature and stirring for 1 h, 3,9-diiodedinaphtho[2,3-*b*:2',3'-*d*] thiophene (**I–DNT–VW**) (309.1 mg, 0.576 mmol) and $PdCl_2$ (dppf)·CH_2Cl_2 (28.5 mg, 0.0349 mmol, 6 mol%) were added. After stirring for 18 h at 80 °C, the reaction was quenched by MeOH. The resulting yellow precipitates were collected by filtration. The resulting material was dissolved in 1,2-dichlorobenzene (500 mL) at 110 °C and subjected to subsequent filtrations through a short pad of silica gel and celite. After removing the solvent *in vacuo*, the yellow solid was further purified by recrystallization from 1,2-dichlorobenzene (110 mL) to afford the titled compound, **Ph–DNT–VW** (180.0 mg, 0.412 mmol, 72% yield) as a yellow solid. ^{1}H-NMR (400 MHz, TCE-d2, 100 °C): δ 7.38 (t, J = 8.0 Hz, 2H, Ar*H*), 7.52 (t, J = 8.0 Hz, 4H, Ar*H*), 7.79 (d, J = 8.0 Hz, 4H, Ar*H*), 7.82 (d, J = 8.8 Hz, 2H, Ar*H*), 8.12 (s, 2H, Ar*H*), 8.15 (d, J = 8.8 Hz, 2H, Ar*H*), 8.30 (s, 2H, Ar*H*), 8.75 (s, 2H, Ar*H*). ^{13}C-NMR could not be determined because of its low solubility. Anal. Calcd for $C_{32}H_{20}S$: C 88.04; H 4.62. Found: C 87.77; H 4.68.

3,9-Bis(p-decylphenyl) dinaphtho[2,3-b:2',3'-d] thiophene (**C_{10}Ph–DNT–VW**)

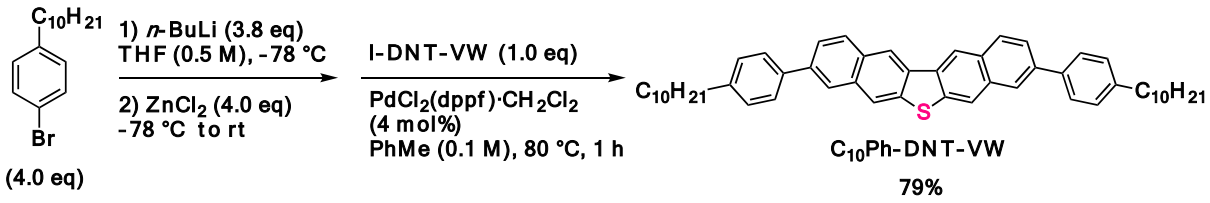

To a solution of *p*-decylphenyl bromide (526.8 mg, 1.77 mmol, 4.0 eq.) in THF (3.54 mL, 0.5 M) was added *n*-BuLi in hexane (1.63 M, 1.04 mL, 1.70 mmol, 3.8 eq.) at –78 °C. After stirring 30 min, $ZnCl_2$ in THF (1 M, 1.77 mL, 1.77 mmol, 4.0 eq.) was added to the white suspension at –78 °C. After warming to the ambient temperature and stirring for 30 min, toluene (4.4 mL, 0.1 M), 3,9-diiodedinaphtho[2,3-*b*:2',3'-*d*] thiophene (**I–DNT–VW**) (237.5 mg, 0.443 mmol) and $PdCl_2(dppf)\cdot CH_2Cl_2$ (14.5 mg, 0.0177 mmol, 4 mol%) were added. After stirring for 1 h at 80 °C, the reaction was quenched by MeOH. The resulting yellow precipitates were collected by filtration. The resulting material was dissolved in 1,2-dichlorobenzene (900 mL) at 120 °C and subjected to subsequent filtrations through a short pad of silica gel and celite. After removing the solvent *in vacuo*, the yellow solid was further purified by recrystallization from 1,2-dichlorobenzene (400 mL) to afford the titled compound, **C_{10}Ph–DNT–VW** (249.7 mg, 0.348 mmol, 79% yield) as a yellow solid. ^{1}H-NMR (400 MHz, TCE-d2, 100 °C): δ 0.89 (t, J = 6.8 Hz, 6H, CH_3), 1.23-1.41 (m, 28H, Ar-CH_2-CH_2-C_7H_{14}), 1.66-1.74 (m, 4H, Ar-CH_2-CH_2), 2.69 (t, J = 7.6 Hz, 4H, Ar-CH_2), 7.30 (d, J = 8.2 Hz, 4H, ArH), 7.67 (d, J = 8.2 Hz, 4H, ArH), 7.79 (d, J = 8.7 Hz, 2H, ArH), 8.07 (s, 2H, ArH), 8.09 (d, J = 8.7 Hz, 2H, ArH), 8.24 (s, 2H, ArH), 8.69 (s, 2H, ArH). ^{13}C-NMR could not be determined because of its low solubility. TOF HRMS (APCI+): Calcd for $C_{52}H_{60}S$ [M+H] 717.4449, found, 717.4477. Anal. Calcd for $C_{52}H_{60}S$: C 87.10; H 8.43. Found: C 87.14; H 8.21.

2. Chemical stability test

Time-dependent UV-vis absorption spectra were measured with a JASCO V-570 spectrometer. Thin films were prepared by vacuum deposition with the thickness of 100 nm on quart substrates.

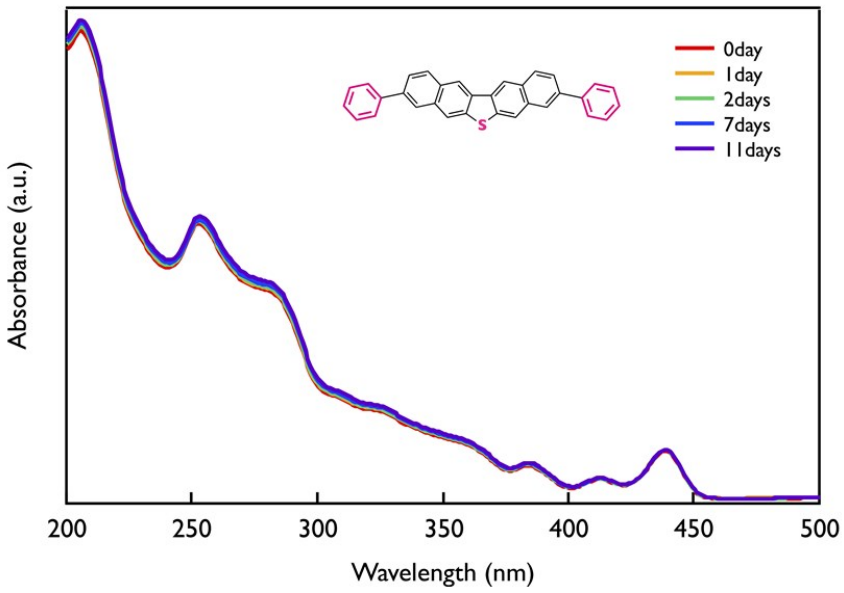

Figure S1. Time-dependent absorption spectra of **Ph–DNT–VW**.

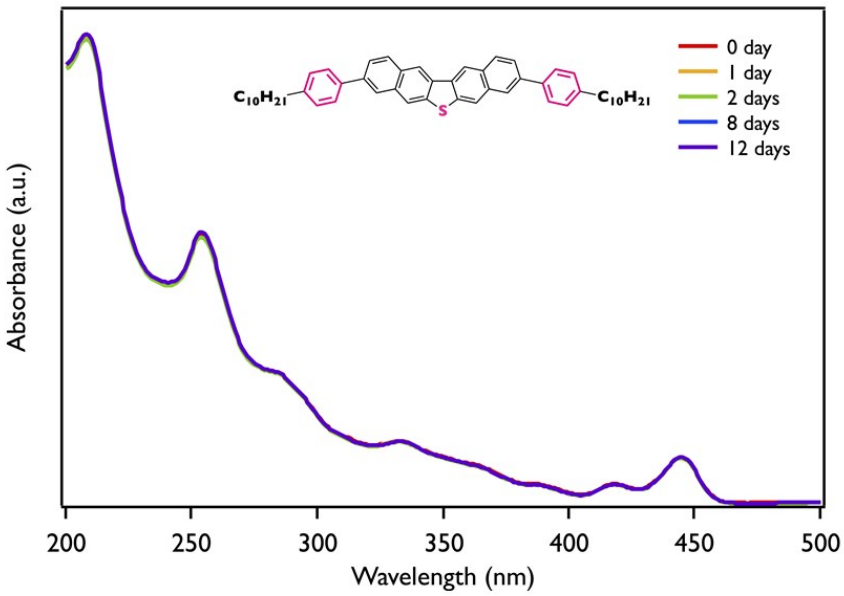

Figure S2. Time-dependent absorption spectra of **C_{10}Ph–DNT–VW**.

3. Thermogravimetric analysis (TGA)

TGA measurement was carried out with a Rigaku Thermo Plus EVO II TG 8121. Sample was placed in aluminum pan and heated at the rate of 5 °C/min, under N_2 purge at a flow rate of 100 mL/min. Al_2O_3 was used as the reference material. Prior to further purification to prepare device grade compounds, their thermal properties were investigated by TGA in the range of room temperature to 800 °C (**C_{10}Ph–DNT–VW**) or 500 °C (**Ph–DNT–VW** and **C_{10}–DNT–VW**). No thermal decomposition was observed in **DNT–V** derivatives in that temperature range, implying that they can be purified by sublimation.

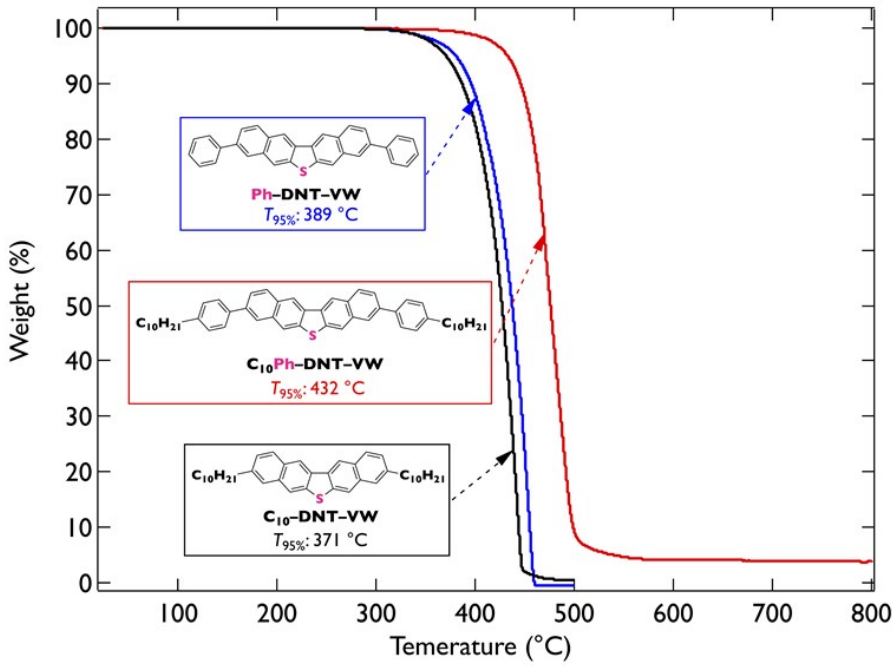

Figure S3. TG plots of **C_{10}Ph–DNT–VW**, **Ph–DNT–VW** and **C_{10}–DNT–VW**.

4. Ionization potential

Photoelectron yield spectroscopy (PYS) was performed on a Sumitomo Heavy Industries Advanced Machinery PYS-202. For PYS measurements, thin films (100 nm) of **C_{10}Ph–DNT–VW** and **Ph–DNT–VW** were thermally evaporated on ITO coated quartz substrates and were measured *in vacuo*. The photoelectron yield spectra are shown in **Figure S4**.

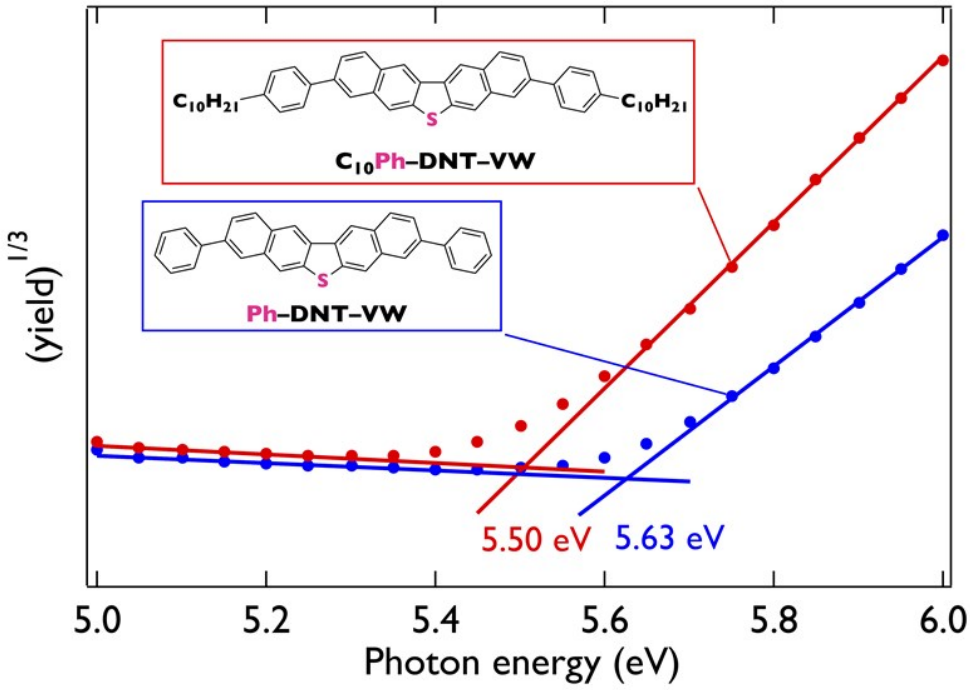

Figure S4. Photoelectron yield spectra of **C_{10}Ph–DNT–VW** and **Ph–DNT–VW** films after light illumination from a D2 lamp *in vacuo*.

5. Single-crystal analysis

Single crystals of **Ph–DNT–VW** and **C_{10}Ph–DNT–VW** were obtained by means of physical vapor transport (PVT) technique[1] and recrystallization from organic solvents, respectively. Single-crystal diffraction data were collected on a Rigaku R-AXIS RAPID II imaging plate diffractometer with Cu Kα radiation (**Table S1**). Improved crystal structure data of **C_{10}–DNT–VW** is also shown in **Table S1**.

Table S1. Crystal data for **Ph–DNT–VW**, **C_{10}Ph–DNT–VW** and **C_{10}–DNT–VW**.

	Ph–DNT–VW	**C_{10}Ph–DNT–VW**	**C_{10}–DNT–VW**
formula	$C_{32}H_{20}S$	$C_{52}H_{60}S$	$C_{40}H_{52}S$
FW	436.57	717.11	564.91
T / K	296	296	296
wavelength / Å	1.54187	1.54187	1.54187
color	yellow	yellow	yellow
crystal size / mm	0.680 × 0.370 × 0.005	1.000 × 0.120 × 0.005	0.360 × 0.120 × 0.005
crystal system	orthorhombic	monoclinic	orthorhombic
space group	*Pna*2$_1$(#33)	*C*2(#5)	*Abm*2(#39)
a / Å	7.5692(2)	88.606(9)	7.8101(7)
b / Å	44.6088(13)	5.9952(6)	72.021(7)
c / Å	6.42563(17)	7.9159(8)	6.0554(6)
α / deg	90	90	90
β / deg	90	90.978(6)	90
γ / deg	90	90	90
V / Å^3	2169.64(11)	4204.4(7)	3406.1(6)
Z	4	4	4
D_X / g cm^{-3}	1.336	1.133	1.102
μ / mm^{-1}	1.449	0.921	1.010
reflections collected	22413	24528	17905
unique reflections	13783	7294	3105
refined parameters	379	478	187
GOF on F^2	1.005	0.927	1.349
$R1$ [$I > 2\sigma(I)$] [a]	0.0425	0.0734	0.1418
w$R2$ (all data) [b]	0.0935	0.1830	0.1590
$\Delta\rho_{min, max}$ / e Å^{-3}	–0.21, 0.15	–0.21, 0.20	–0.55, 0.36
CCDC number	2010669	2010670	2010721

[a] $R1 = \Sigma \, ||Fo|-|Fc|| \, / \, \Sigma \, |Fo|$, [b] $wR2 = [\Sigma \, (w(Fo^2-Fc^2)^2/\Sigma \, w(Fo^2)^2)]^{1/2}$

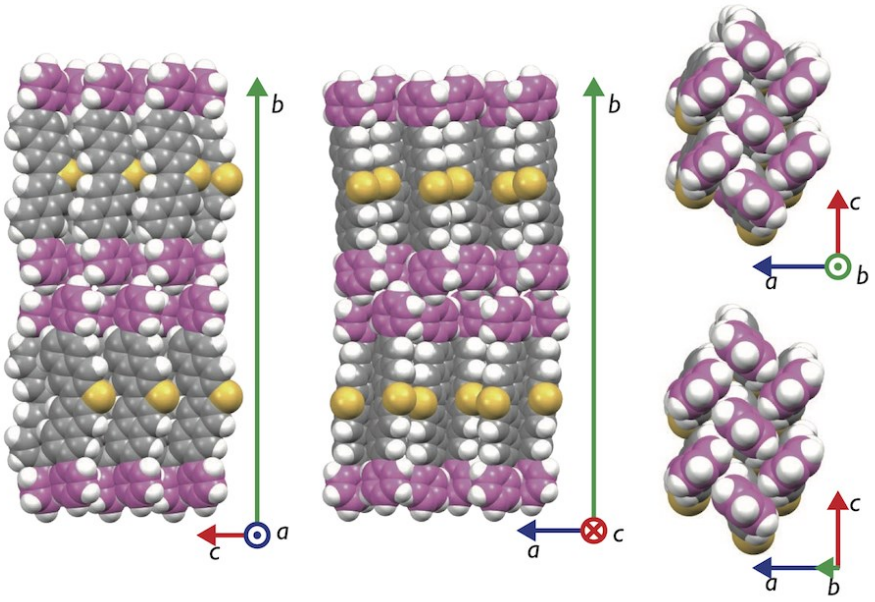

Figure S5. Packing structures of **Ph–DNT–VW** in space filling style viewed from various directions.

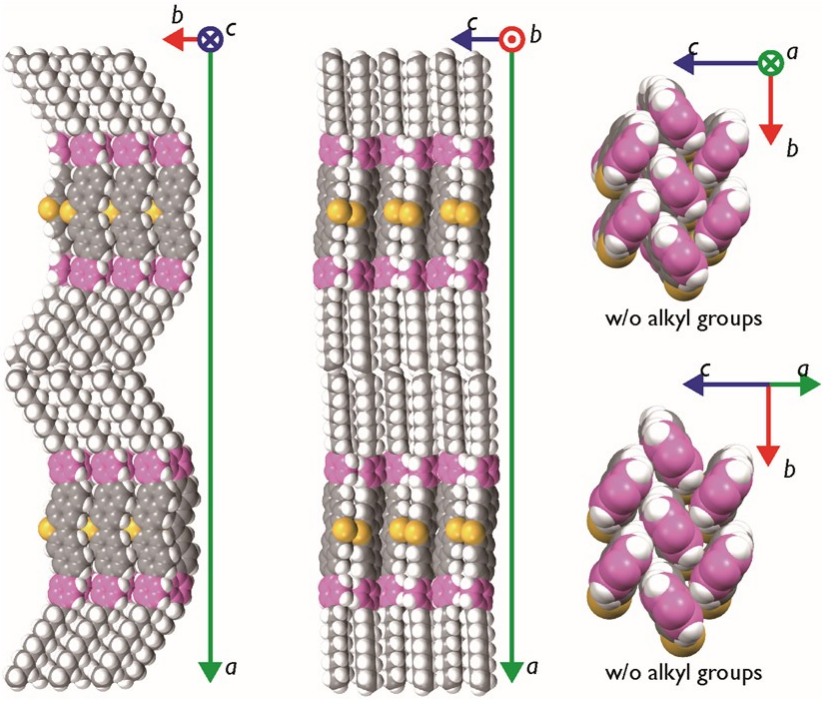

Figure S6. Packing structures of **C_{10}Ph–DNT–VW** in space filling style viewed from various directions.

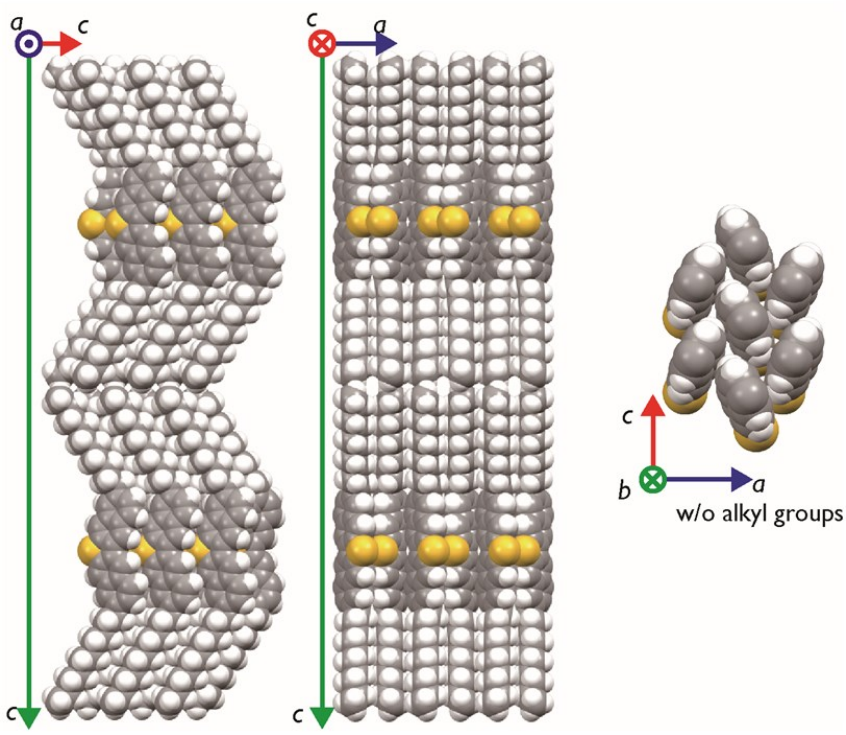

Figure S7. Packing structures of C_{10}**–DNT–VW** in space filling style viewed from various directions.

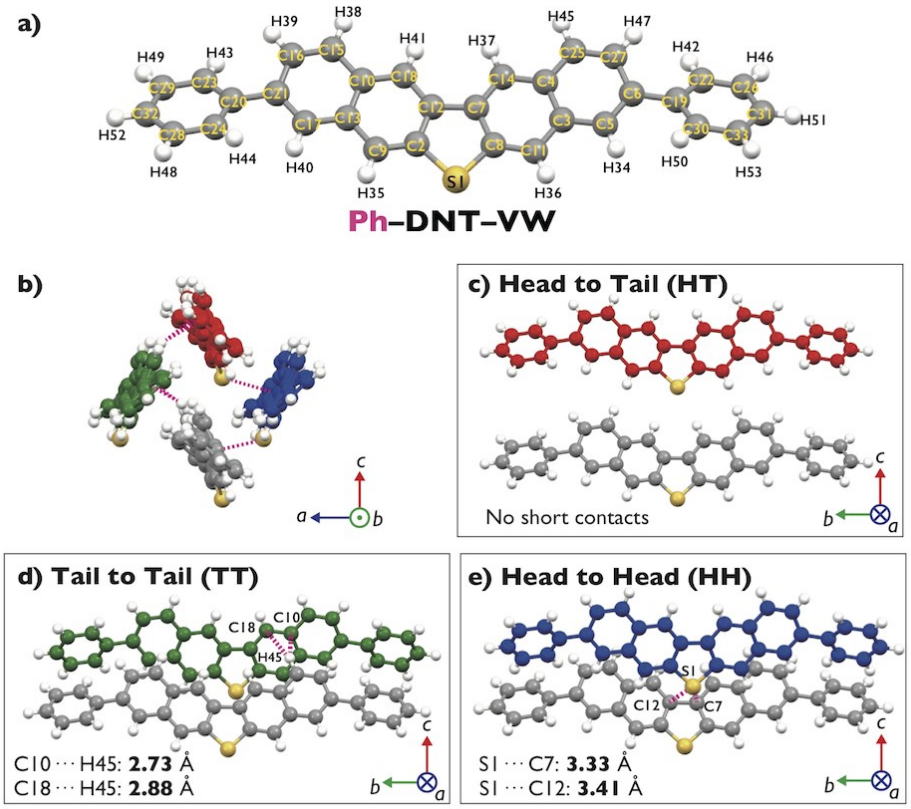

Figure S8. Intermolecular interactions and short contacts of **Ph–DNT–VW**.

The herringbone packing structure exhibits two predominant types of short C–H···π and S···π interactions, which are shorter than the sum of van der Waals radii for hydrogen (1.20 Å), carbon (1.70 Å), and sulfur (1.80 Å).[2] Specifically, short contacts along *c*-axis (S1···C7: 3.33 Å, S1···C12: 3.41 Å) are observed due to S···π interactions between the inner thiophenes, and short contacts the inner phenyl groups (C10···H45: 2.73 Å, C18···H45: 2.88 Å) are observed.

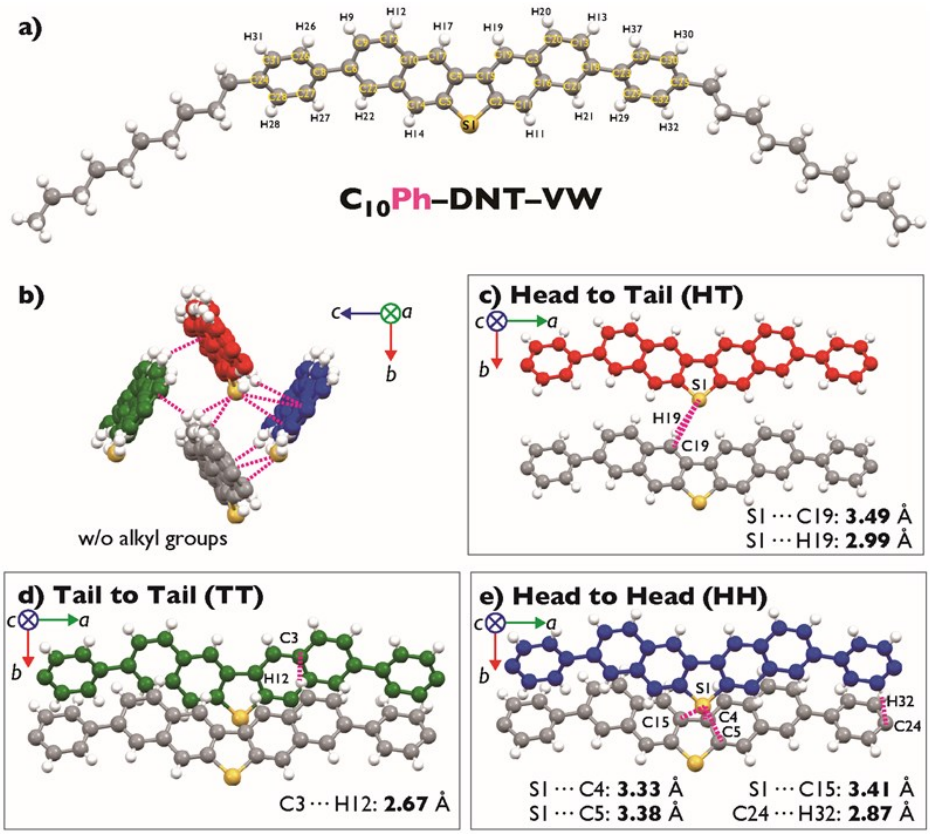

Figure S9. Intermolecular interactions and short contacts of **C_{10}Ph–DNT–VW**.

The herringbone packing structure exhibits two predominant types of short C–H···π and S···π interactions. Specifically, short contacts along *b*-axis (S1···C19: 3.49 Å, S1···H19: 2.99 Å) are observed due to S···π interactions between the inner thiophenes, and short contacts between substituted phenyl groups (C24···H32: 2.87 Å) are observed as expected.

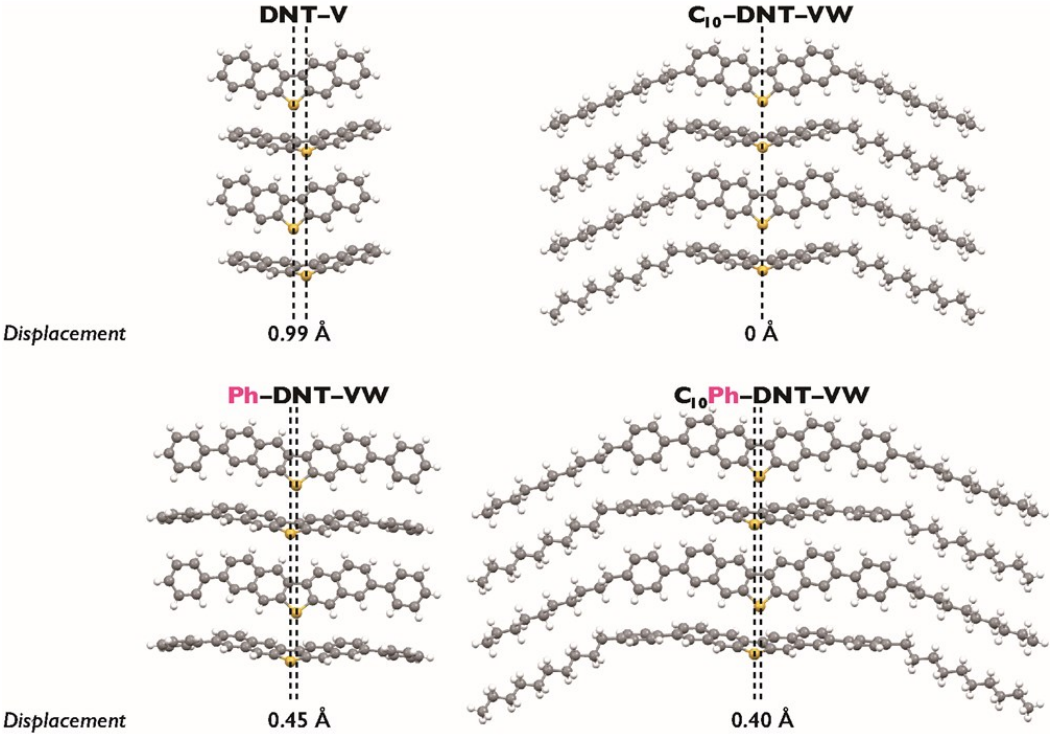

Figure S10. Molecular displacements of **DNT–V**, **C_{10}–DNT–VW**, **Ph–DNT–VW** and **C_{10}Ph–DNT–VW** in the transverse direction.

6. Theoretical Calculation: transfer integrals and band calculations

Based on the crystal structures, transfer integral (t) values of the HOMOs between neighboring molecules were calculated by density functional theory at the PBEPBE/6-31G(d) level.

To further understand the carrier transporting capabilities in the bulk state, the electronic band structures of **Ph–DNT–VW**, **C_{10}Ph–DNT–VW** and **C_{10}–DNT–VW** based on the packing structures with 2-dimensional periodic boundary condition were also calculated. . The energies are plotted and labeled as Γ = (0, 0, 0), S = (0.5, 0.5, 0), T = (0, 0.5, 0.5), U = (0.5, 0, 0.5), X = (0.5, 0, 0), Y = (0, 0.5, 0), Z = (0, 0, 0.5) in the crystallographic coordinates. Effective hole masses were calculated as $m^* = \hbar^2\left(\frac{\partial^2 E(k)}{\partial k^2}\right)^{-1}$ along column directions and transverse directions.

Table S2. The transfer integral (t) values of the HOMOs between neighboring molecules.

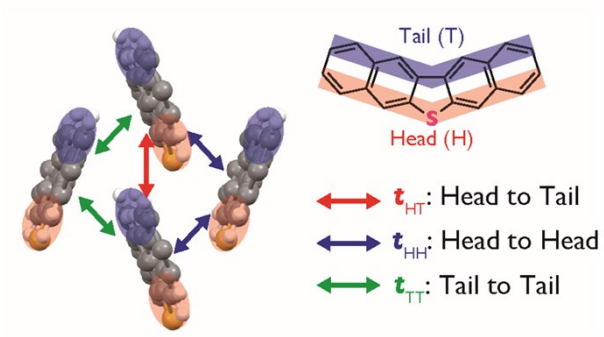

Material	Transfer integral (t, meV)		
	t_{HT}	t_{HH}	t_{TT}
Ph–DNT–VW	+33	–50	–33
C_{10}Ph–DNT–VW	+40	–45	–32
C_{10}–DNT–VW	+43	–69	–35
DNT–V	+37	–46	–13

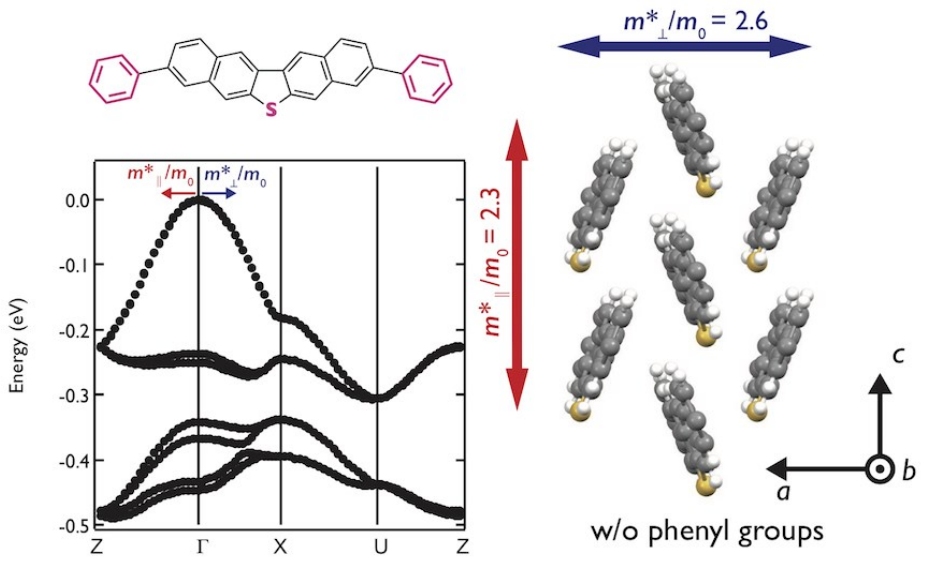

Figure S11. Electric band structure and effective masses of **Ph–DNT–VW**.

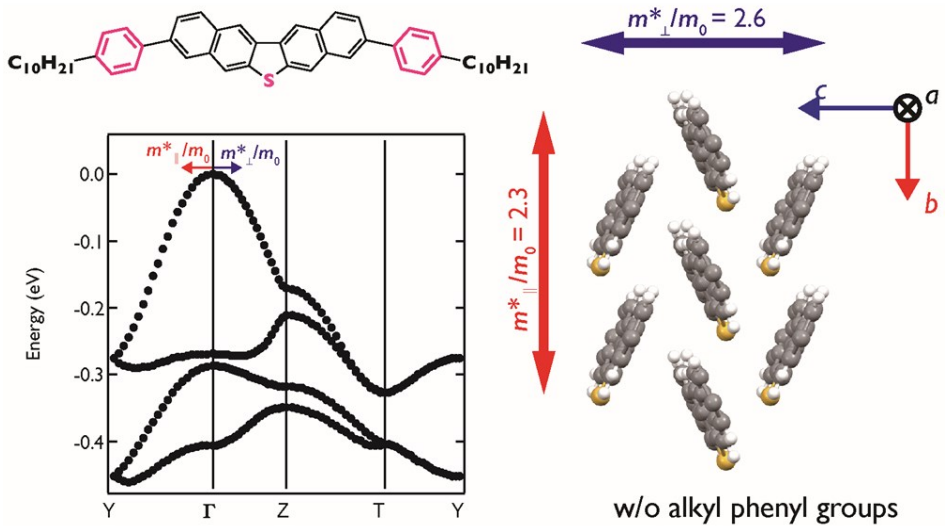

Figure S12. Electric band structure and effective masses of **C_{10}Ph–DNT–VW**.

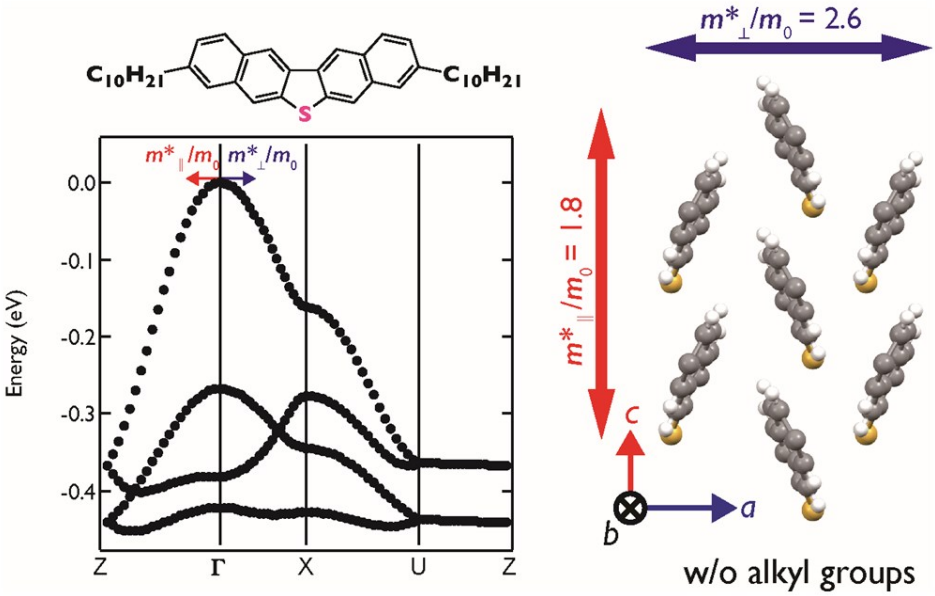

Figure S13. Electric band structure and effective masses of **C_{10}–DNT–VW**.

7. Solubility test

To a weighed sample of around 0.2 - 4 mg was added 20 μL of 3-phenoxytoluene, repeatedly. The resulting suspension was heated at 80 °C. The weight of sample was planed so that the volume of resulting solution would be 300 mg at least. The results are summarized in **Table S3**.

Table S3. Solubility of **DNT–V** derivatives in 3-phenoxytoluene at 80 °C.

Material	Solubility in 3-phenoxytoluene (wt%) at 80 °C
Ph–DNT–VW	<0.0005
C_{10}Ph–DNT–VW	0.0058
C_{10}–DNT–VW	1.1
DNT–V	0.50

8. Two-probe OFET device fabrications and evaluation procedure

Two-probe organic field-effect transistors using organic semiconducting single crystalline films were fabricated with the lamination method for **Ph–DNT–VW** and the edge-casting method[3] for **C_{10}Ph–DNT–VW**. The surfaces of a heavily-doped silicon wafers with thermally-oxidized SiO_2 (500 nm) were pretreated with self-assembled monolayers (SAMs) prior to each method; heptadecafluorodecyl triethoxysilane (FDTS-SAM) for the lamination method and *β*-phenylethyl trimethoxysilane (*β*-PTS-SAM) for the edge-casting method. Onto the FDTS-SAM treated substrates, **Ph–DNT–VW** crystals, which were grown by the PVT technique, were softly laminated. On the other hand, on the *β*-PTS-SAM treated substrates, a droplet of solution of **C_{10}Ph–DNT–VW** was put at the edge of a liquid-sustaining piece. The organic crystalline films grew on top of the solution surface, during the solvent evaporated from opposite side of the sustaining piece, to land softly on the substrate.[3] After removing the sustaining piece, the film on the substrate was dried under heating in vacuum. For **C_{10}Ph–DNT–VW**, 0.03 wt% 3-phenoxytoluene solution was dropped on the substrate at 80 °C, and the film was dried at 80 °C in vacuum for 10 hours.

Onto the both crystalline films, F_4–TCNQ (2 nm) and Au (40 nm) were thermally deposited through a shadow mask to construct bottom-gate-top-contact architecture. Finally, crystals were shaped into rectangular channels by laser etching to determine channel length (L) and width (W) accurately for evaluation of mobility. The channel directions were set to be along the crystal growth directions, and it was confirmed by transmission XRD that the channel directions of devices are almost along the column direction of the herringbone packing structures (Figure S8d, e, f, Figure S9d, e, f). In the device, SiO_2 layer acts as a gate insulator, doped silicon as a gate electrode, and Au as contact electrodes (source and drain electrode). The layer of F_4–TCNQ, electron-accepting material, was introduced between the organic semiconductor and contacts to reduce parasitic contact resistance.

Transistor characterizations were carried out under ambient air using a Keithley 4200 semiconductor parameter analyzer with source measurement units (SMUs). Transistor characteristics for **Ph–DNT–VW** single crystals grown via PVT technique, and **C_{10}Ph–DNT–VW** single crystals grown via edge-casting method are shown in **Figure S14** and **Figure S15.**, respectively. After checking small hysteresis in transfer curve and saturation of drain current in output characteristics, field-effect mobilities ($\mu_{2\text{-probe}}$) in the saturation regime were evaluated using the following equation:

$$I_D = \frac{WC}{2L} \mu_{2-probe} (V_G - V_{th})^2$$

Where C is the capacitance of gate insulator and V_{th} is the threshold voltage. The highest mobility values are summarized in main text.

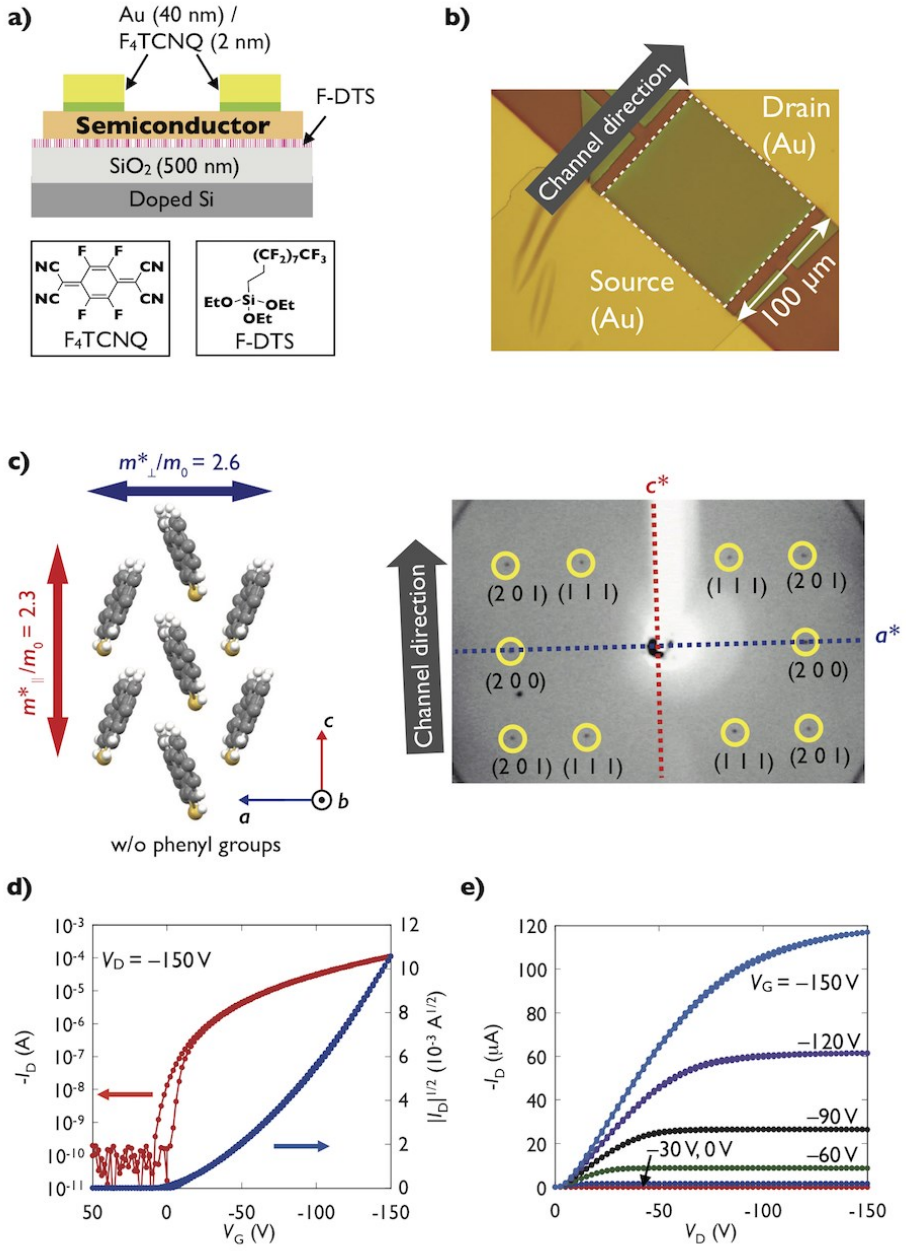

Figure S14. OFET characteristics of **Ph–DNT–VW** with the channel direction which is parallel to the column direction. a) Device structure and chemical structure of F_4-TCNQ and FDTS, b) the microscopic image of device, c) assigned Laue spots of in-plane X-ray diffraction of the crystallin film with the channel direction (BL-8A Photon Factory, KEK) and the crystal structure with lattice directions output characteristics, d) transfer and e) output characteristics of OFET.

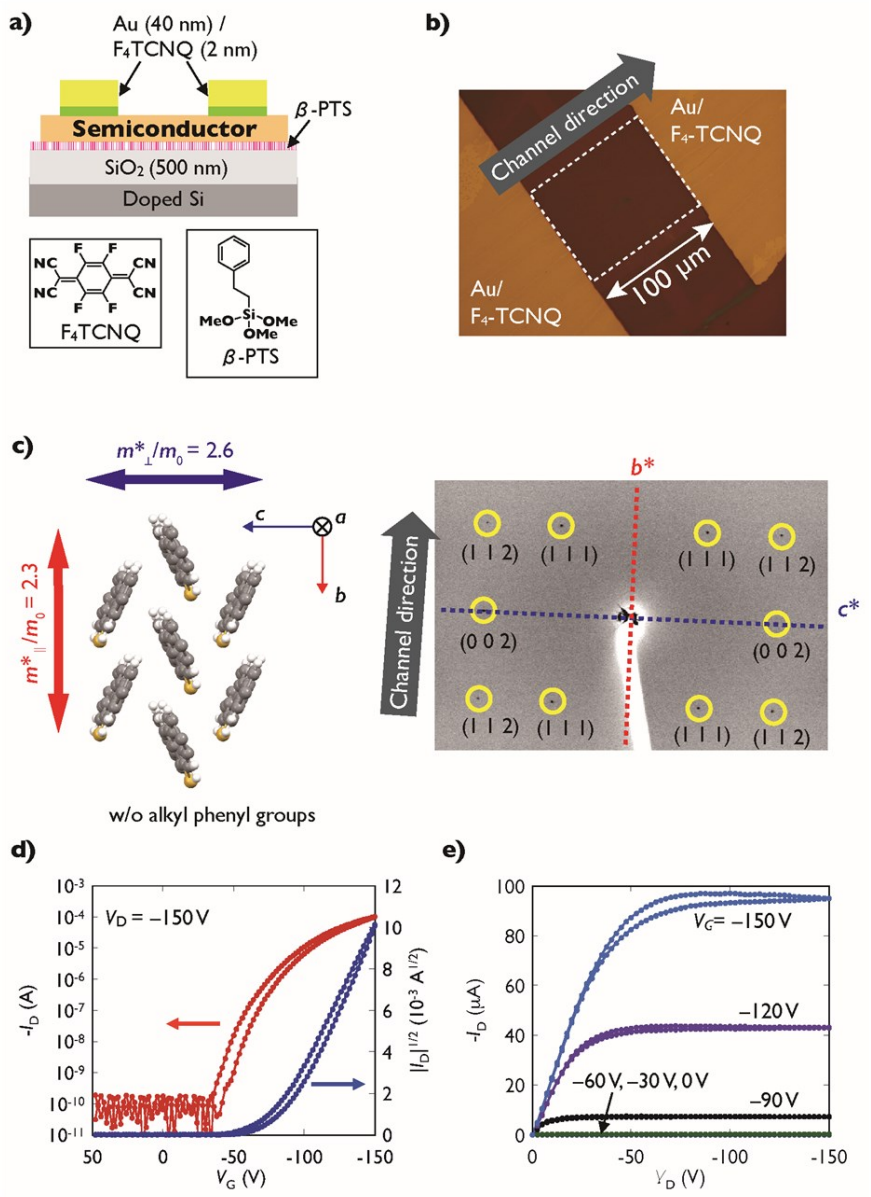

Figure S15. OFET characteristics of **C_{10}Ph–DNT–VW** with the channel direction which is parallel to the column direction. a) Device structure and chemical structure of F_4-TCNQ and FDTS, b) the microscopic image of device, c) assigned Laue spots of in-plane X-ray diffraction of the crystallin film with the channel direction (BL-8A Photon Factory, KEK) and the crystal structure with lattice directions output characteristics, d) transfer and e) output characteristics of OFET.

9. Temperature-dependent mobility measurement

Four-probe OFETs using single crystalline films were fabricated with the lamination method for **DNT–V** and **Ph–DNT–VW** and the edge-casting method[3] for **C_{10}Ph–DNT–VW** and **C_{10}–DNT–VW**. The surfaces of a heavily-doped silicon wafers with thermally-oxidized SiO_2 (100 nm) were pretreated with self-assembled monolayers (SAMs) prior to each method; heptadecafluorodecyl triethoxysilane (FDTS-SAM) for the lamination method and *β*-phenylethyl trimethoxysilane (*β*-PTS-SAM) for the edge-casting method. Onto the FDTS-SAM treated substrates, **DNT–V** and **Ph–DNT–VW** crystals, which were grown by the PVT technique, [3] were softly laminated. On the other hand, on the *β*-PTS-SAM treated substrates, droplets of solution of **C_{10}Ph–DNT–VW** and **C_{10}–DNT–VW** was put at the edge of a liquid-sustaining piece. The organic crystalline films grew on top of the solution surface, during the solvent evaporated from opposite side of the sustaining piece, to land softly on the substrate.[3] After removing the sustaining piece, the film on the substrate was dried under heating in vacuum. For **C_{10}Ph–DNT–VW**, 0.03 wt% 3-phenoxytoluene solution was dropped on the substrate at 80 °C, and the film was dried at 80 °C in vacuum for 10 hours For **C_{10}–DNT–VW**, 0.01 wt% anisole solution was dropped on the substrate at 45 °C, and the film was dried at 40 °C in vacuum for 10 hours.

Onto the crystalline films, F_4–TCNQ (2 nm) and Au (40 nm) were thermally deposited through a shadow mask. In the device, SiO_2 layer acts as a gate insulator, doped silicon as a gate electrode, and Au as contact electrodes (source and drain electrode). The layer of F_4–TCNQ, electron-accepting material, was introduced between the organic semiconductor and contacts to reduce parasitic contact resistance.

Laser etching was performed (V-Technology Co., Ltd., Callisto (266 nm)) for crystalline layer to form a precise four-probe architecture. The resulting voltage probes are shown in **Figure S16.** a). The channel length (*L*) and width (*W*) were 240 μm and 60 μm, respectively. Four probes were mounted in between the source and drain electrodes, where the distance between two longitudinal probes along the channel length (defined as L^*) was designed to be 120 μm.

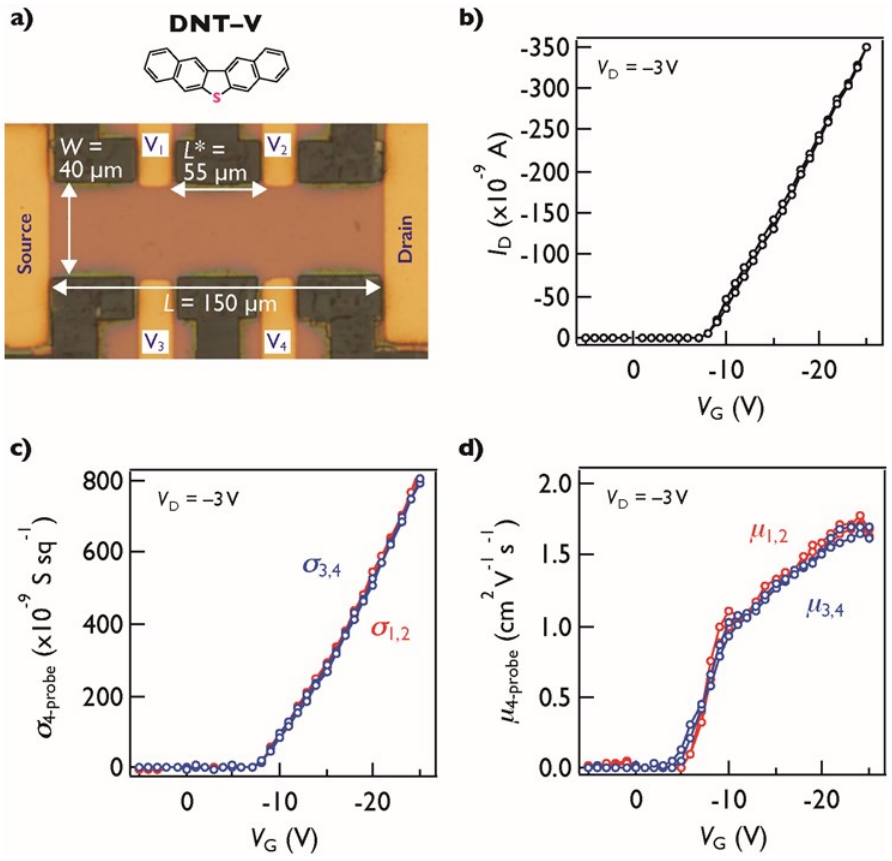

Figure S16. a) Optical microscopic image of four-probe transistor using solution-grown crystalline film of **DNT–V** and b) its drain current (I_D) as a function of gate voltage (V_G), c) four-probe sheet conductivity ($\sigma_{1,2} = \frac{I_D \quad L^*}{V_2 - V_1 W}$ and $\sigma_{3,4} = \frac{I_D \quad L^*}{V_4 - V_3 W}$) as a function of gate voltage (V_G), d) V_G-dependent four-probe mobility ($\mu_{1,2} = \frac{1}{C_i}\frac{\partial \sigma_{1,2}}{\partial V_G}$ and $\mu_{3,4} = \frac{1}{C_i}\frac{\partial \sigma_{3,4}}{\partial V_G}$). The four-probe mobility shows good saturation in the high V_G region.

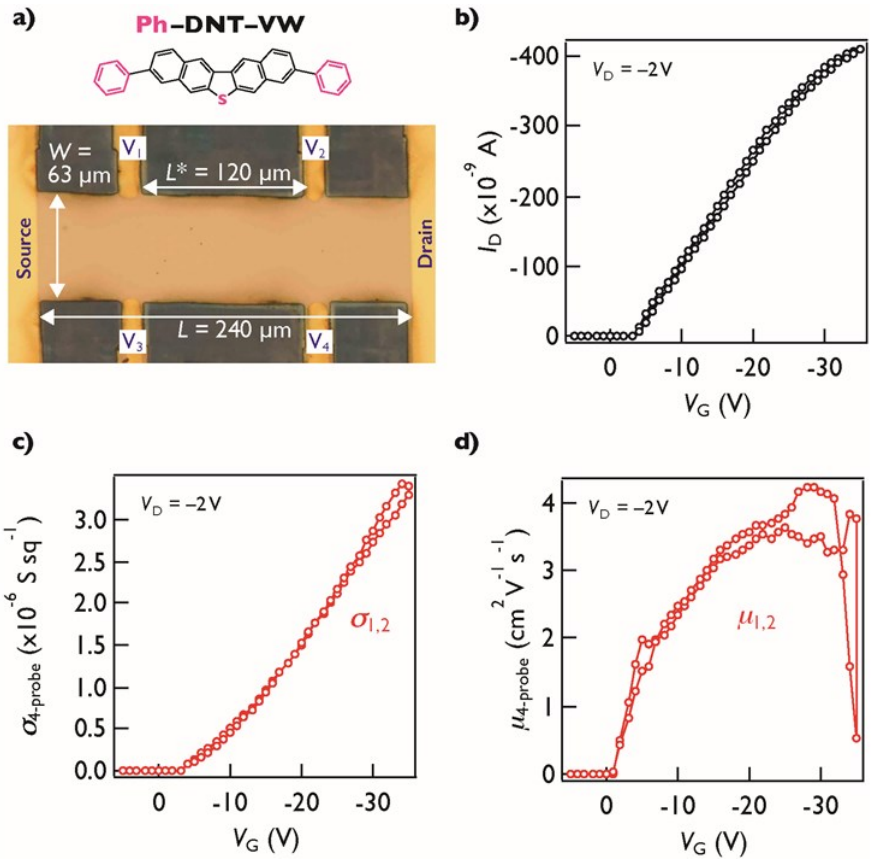

Figure S17. a) Optical microscopic image of four-probe transistor using solution-grown crystalline film of **Ph–DNT–VW** and b) its drain current (I_D) as a function of gate voltage (V_G), c) four-probe sheet conductivity ($\sigma_{1,2} = \frac{I_D}{V_2 - V_1} \frac{L^*}{W}$) as a function of gate voltage (V_G), d) V_G-dependent four-probe mobility ($\mu_{1,2} = \frac{1}{C_i} \frac{\partial \sigma_{1,2}}{\partial V_G}$). The four-probe mobility shows good saturation in the high V_G region.

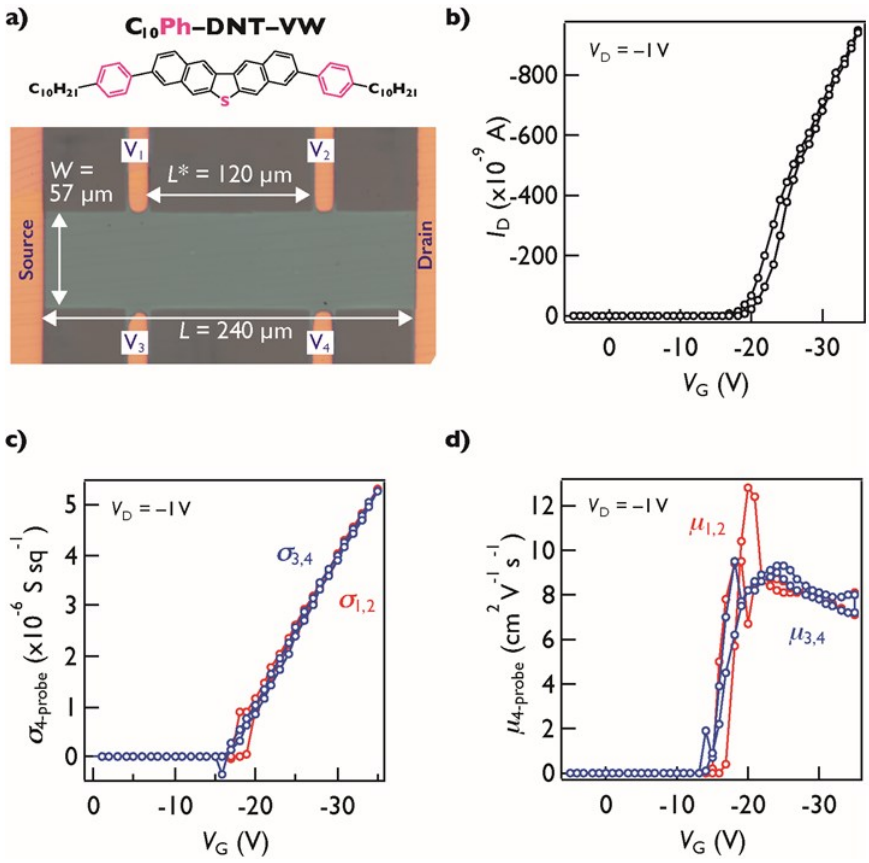

Figure S18. a) Optical microscopic image of four-probe transistor using solution-grown crystalline film of **C_{10}Ph–DNT–VW** and b) its drain current (I_D) as a function of gate voltage (V_G), c) four-probe sheet conductivity ($\sigma_{1,2} = \frac{I_D \quad L^*}{V_2 - V_1 W}$ and $\sigma_{3,4} = \frac{I_D \quad L^*}{V_4 - V_3 W}$) as a function of gate voltage (V_G), d) V_G-dependent four-probe mobility ($\mu_{1,2} = \frac{1}{C_i}\frac{\partial \sigma_{1,2}}{\partial V_G}$ and $\mu_{3,4} = \frac{1}{C_i}\frac{\partial \sigma_{3,4}}{\partial V_G}$). The four-probe mobility shows good saturation in the high V_G region.

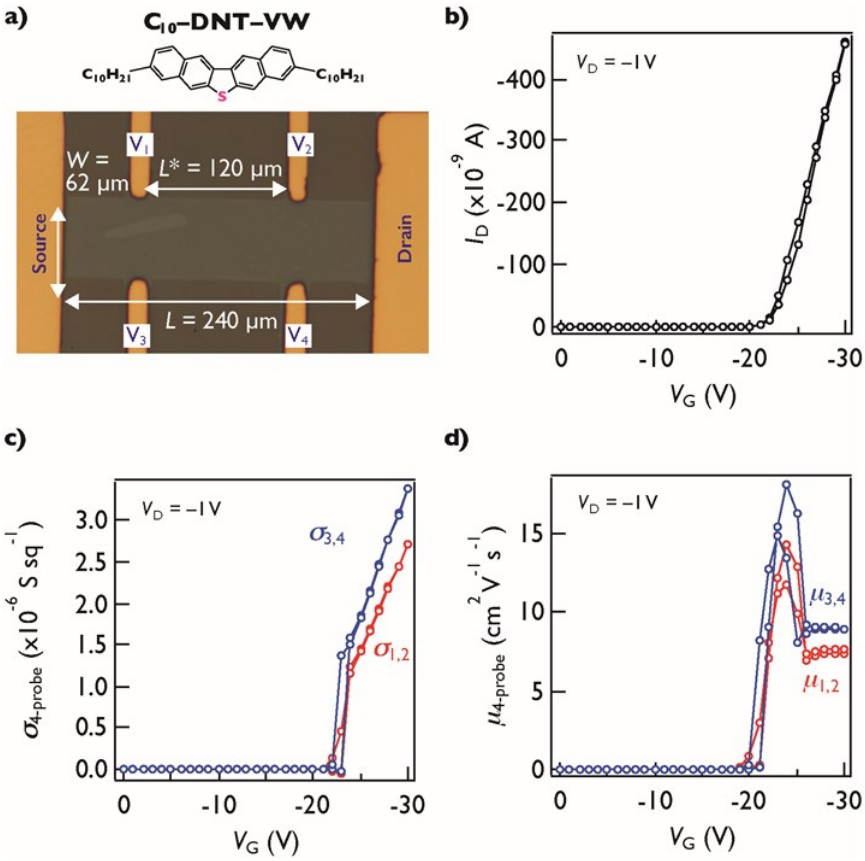

Figure S19. a) Optical microscopic image of four-probe transistor using solution-grown crystalline film of **C_{10}–DNT–VW** and b) its drain current (I_D) as a function of gate voltage (V_G), c) four-probe sheet conductivity ($\sigma_{1,2} = \frac{I_D \quad L^*}{V_2 - V_1 W}$ and $\sigma_{3,4} = \frac{I_D \quad L^*}{V_4 - V_3 W}$) as a function of gate voltage (V_G), d) V_G-dependent four-probe mobility ($\mu_{1,2} = \frac{1}{C_i}\frac{\partial \sigma_{1,2}}{\partial V_G}$ and $\mu_{3,4} = \frac{1}{C_i}\frac{\partial \sigma_{3,4}}{\partial V_G}$). The four-probe mobility shows good saturation in the high V_G region.

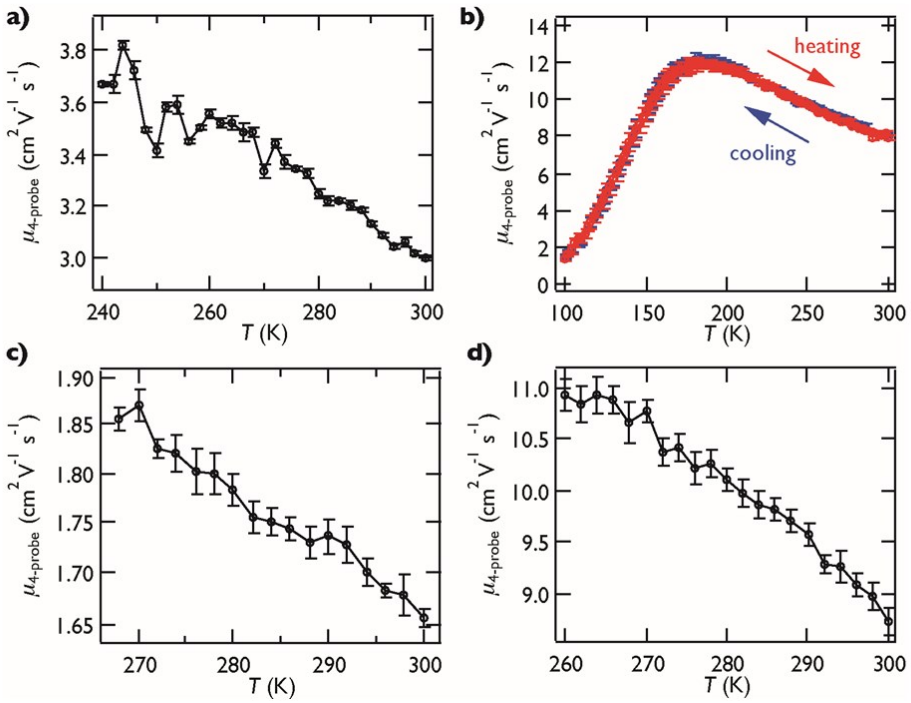

Figure S20. Temperature dependence of four-probe mobiliy. a) **Ph–DNT–VW**, b) **C_{10}Ph–DNT–VW**, c) **DNT–V** and d) **C_{10}–DNT–VW**.

10. Thermal stress test for C_{10}Ph–DNT–VW

Device preparation

For thermal stress test, OFETs using **C_{10}Ph–DNT–VW** single crystalline films were fabricated with the edge-casting method. [3] The surfaces of a heavily-doped silicon wafers with thermally-oxidized SiO_2 (100 nm) were pretreated with self-assembled monolayer (SAM); *β*-phenylethyl trimethoxysilane (*β*-PTS-SAM) prior to the edge-casting method. On the *β*-PTS-SAM treated substrates, a droplet of 0.03 wt% 3-phenoxytoluene solution of **C_{10}Ph–DNT–VW** was put at the edge of a liquid-sustaining piece on the substrate at 80 °C, and after removing the sustaining piece, the film was dried at 80 °C in vacuum for 10 hours to remove the solvent. After drying, crystalline films were annealed at 180 °C under N_2 for 10 min. The heating and cooling rates were set to be 0.2 K/min.

Onto the crystalline films, Au (40 nm) was thermally deposited through a shadow mask. In the device, SiO_2 layer acts as a gate insulator, doped silicon as a gate electrode, and Au as contact electrodes (source and drain electrode). The layer of F_4–TCNQ was not depositted on the device for thermal stress test to exclude the effect of F_4–TCNQ's change at high temperature. On the other hand, F_4–TCNQ (3 nm) was thermally depositted on the other device to evaluate the mobility of pre-annealed film properly.

Laser etching was performed (V-Technology Co., Ltd., Callisto (266 nm)) for crystalline layer to form rectangular channels to determine channel length (*L*) and width (*W*) accurately.

Transistor characterizations were carried out under ambient air using a Keithley 4200 semiconductor parameter analyzer with source measurement units (SMUs).

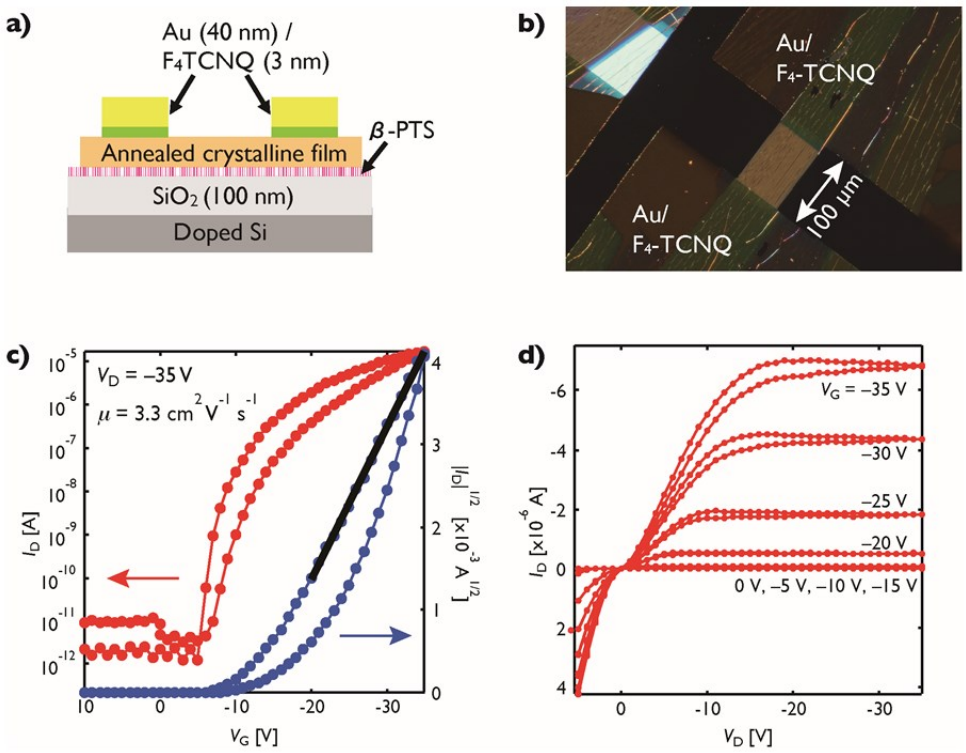

Figure S21. OFET characteristics of pre-annealed (180 °C) crystalline film of **C_{10}Ph–DNT–VW** with F_4–TCNQ. a) Device structure, b) the microscopic image of device, c) transfer and d) output characteristics of OFET.

Thermal stress test

The device for thermal stress test (not using the F_4-TCNQ) was heated at 60 °C, 100 °C, 140 °C, 160 °C and 180 °C for 5 min in a N_2-filled oven. The heating and cooling rates were 0.2 K/min. The device performance was evaluated under ambient air at room temperature. Using the same device for thermal stress test, the heating and cooling processes were repeated up to 180 °C.

Figure S22. Microscopic images of **C_{10}Ph–DNT–VW** single-crystal transistor for thermal stress test after 100 °C annealing a) without and b) with crossed-Nicol, and after 180 °C annealing c) without and d) with crossed-Nicol.

Transmission XRD measurement of crystalline film at high temperature

To obtain the crystal structure information of **C_{10}Ph–DNT–VW** single crystalline and annealed films at high temperature, transmission XRD measurement were performed with blowing temperature-controled N_2 gas. The wave length of X-ray was 0.6887 Å.

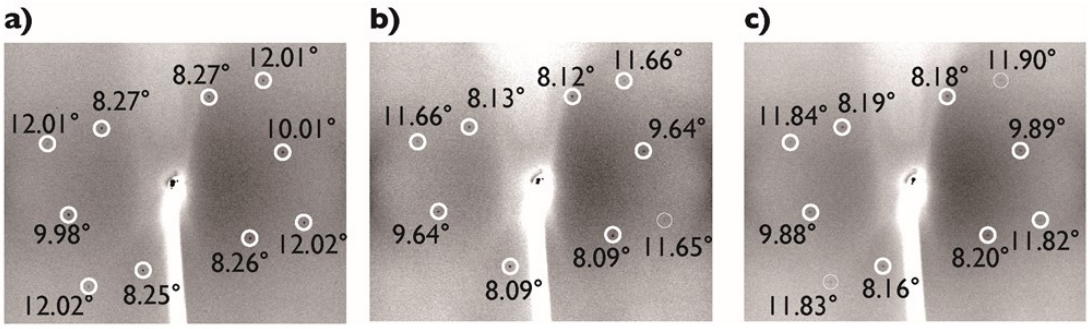

Figure S23. In-plane X-ray diffraction of **C_{10}Ph–DNT–VW** single crystalline film. a) Before heating, b) 180 °C, c) after 180 °C heating (room temperature).

11. Observation of annealed film of C_{10}–DNT–VW

To observe the film morphology of **C_{10}–DNT–VW** at high temperature, a crystalline thin film of **C_{10}–DNT–VW** was prepared by the edge-casting method. On β-PTS-SAM treated silicon wafer, a droplet of 0.01 wt% anisole solution of **C_{10}–DNT–VW** was put at the edge of a liquid-sustaining piece on the substrate at 45 °C, and after removing the sustaining piece, the film was dried at 40 °C in vacuum for 10 hours to remove the solvent. After drying, the crystalline films were annealed at 150 °C and 180 °C under N_2 for 10 min.

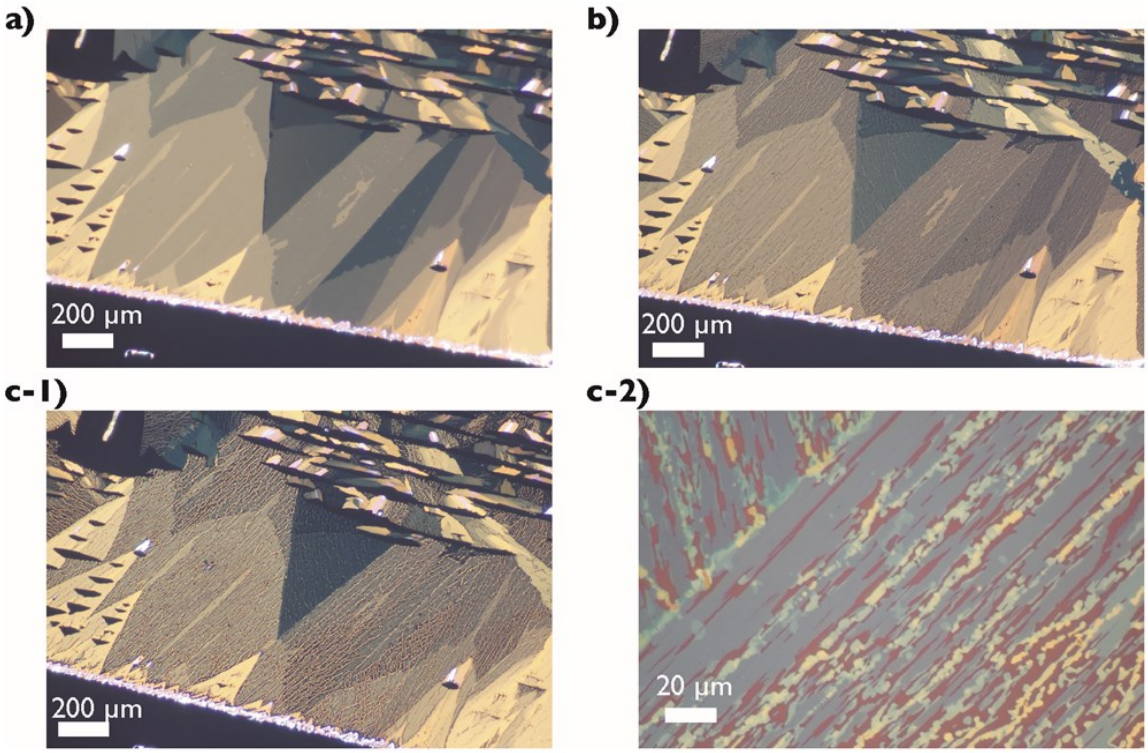

Figure S24. Microscopic images of **C_{10}–DNT–VW** single crystalline film after 100 °C annealing a) before annealing, b) after 150 °C annealing and c) after 180 °C annealing.

12. References

[1] C. Kloc, P. G. Simpkins, T. Siegrist and R. A. Laudise, *J. Cryst. Growth*, 1997, **182**, 416.

[2] A. Bondi, *J. Phys. Chem.*, 1964, **68**, 441.

[3] T. Uemura, Y. Hirose, M. Uno, K. Takimiya and J. Takeya, *Appl. Phys. Express*, 2009, **2**, 111501.